Pergamon

0956-7151(94)00349-1

Acta metall. mater. Vol. 43, No. 4, pp. 1559–1568, 1995

0956-7151/95 $9.50 + 0.00

A SIMULATION OF THE NiO/Ag INTERFACE WITH POINT DEFECTS

D. M. DUFFY, J. H. HARDING and A. M. STONEHAM
AEA Industrial Technology, Harwell Laboratory, Oxfordshire, OX11 0RA, England

(Received 18 June 1994)

Abstract—The NiO/Ag interface has been modelled using established simulation techniques, which have been modified to include the image interactions between the oxide ions and the induced charge in the metal. The energies of point defects near the interface were calculated and it was found that the surface rumpling was such that defects with a negative net charge were favoured. This will result in a space charge layer with excess cation vacancies which will cancel the interfacial potential. A low energy interface was modelled in which the cation sub-lattice of the second oxide plane was saturated with vacancies and Ni^{3+} ions. Such a structure may be responsible for the observed excess of oxygen near the NiO/Ni interface, and also for the low wetting angles of metals on NiO, compared with MgO.

1. INTRODUCTION

Metal/oxide interfaces have attracted considerable attention in recent years and simple interfaces have been studied, using both experimental and theoretical techniques, in order to gain insight into the fundamental processes involved in the adhesion of such interfaces. This interest reflects the significance of metal/oxide interfaces in many technological processes, adhesive protective coatings, catalyst support and electronic packaging, representing some examples. In our work we aim to identify the general features of metal/oxide interfaces and explore how these can be used to control adhesion and other relevant properties of interfaces.

In a recent paper [1] we described a method for the calculation of the structure of metal/oxide interfaces which included the interactions between the oxide ions and the image charges induced in the metal. The classical image interaction is screened by the restriction of the induced charge distribution, caused by the finite Fermi wave-vector of the metal [2]. Other significant interactions include the Coulomb interactions between the ionic charges, the short range interactions between the oxide ions and the short range interactions between the oxide ions and the metal cores. The energy required to immerse the oxide ions in the metal jellium is also introduced into the calculation. These interactions are included in well established atomistic simulation techniques and form the basis of our model of the metal/oxide interface.

In our earlier paper [1] we presented results for the MgO/Ag interface. This interface is often chosen as a model interface for metal/oxide interfaces because the two materials are effectively non-reactive and the lattice parameters are a close match. MgO has a very low intrinsic defect concentration and the defect structure of this oxide is generally determined by the impurity content. NiO has the same structure and a similar lattice parameter to MgO, though this oxide has a higher dielectric constant and a greater tendency to disorder. In this paper we calculate the structure of the NiO/Ag interface, with and without point defects, and the results are compared with the earlier calculations on the MgO/Ag interface. The effect of charged defects on the properties of the interface, such as the interfacial energy and the wetting angles, is discussed, since early work suggested the disorder was an important feature [3, 4].

The structure of the MgO/Ag interface has also been calculated using electronic structure calculations [5, 6]. Such calculations provide information about the electronic densities at the interface, in addition to interfacial energies and dilations. They are, however, restricted to simple, non-defective interfaces and they require powerful computers. Our approach is complementary to the LDA calculations as it provides a method for examining a range of interfaces, with and without point defects, using only minimal computing power. Under some circumstances, in particular when significant electron transfer occurs, the calculations are beyond the scope of our model and a full electronic calculation is required. Fortunately such situations are rare and our approach provides a powerful, cheap method for studying a variety of metal/oxide interfaces.

2. THE STRUCTURE OF THE NiO/Ag INTERFACE

2.1. The simulation method

The structure of the interface was calculated using the Harwell MIDAS code [7], in which the two-

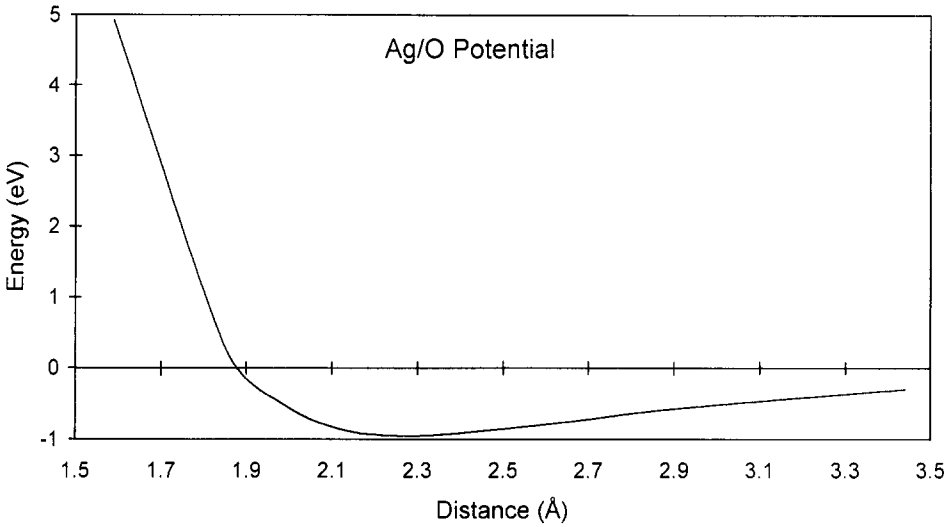

Fig. 1. The calculated potential for the Ag/O interaction.

dimensional periodicity of the structure is utilized for the calculation of the long range Coulomb interactions between the charged ions. The program has been modified to include the interaction between the ionic charges and the induced image charges in the metal. The classical image interaction diverges as the ionic charges approach the image plane and this, in the past, led to problems in obtaining a balance between the attractive image interactions and the repulsive short range interactions. In real metals, however, the induced charge distribution is restricted by the finite Fermi wave vector. The charge distribution induced in the metal, under the conditions where the fluctuations are restricted to those with wave-vectors shorter than the Fermi wave-vector, has been calculated by Willis and the details are presented in an appendix of an earlier paper [2]. Introducing this restriction into the induced charge distribution effectively screens the image interaction and removes the unphysical divergence at the image plane.

The short range interactions between the oxide ions were taken to be the empirical shell model potentials of Sangster and Stoneham [8]. These potentials have been used for a wide range of calculations in bulk NiO, at grain boundaries [9] and at surfaces [10], and good agreement has been found with the available experimental data. The interaction between the oxygen ions and the silver atoms was calculated for the previous work on MgO, using the Dirac–Fock methods developed by Wood and Pyper [11, 12]. The resulting interactions are fitted to a cubic spline

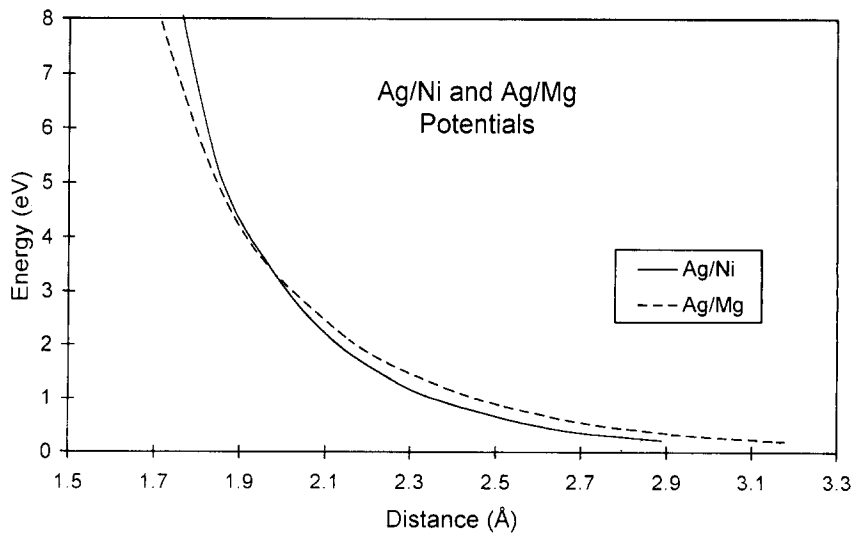

Fig. 2. The calculated potentials for the Ag/Ni and Ag/Mg interactions.

potential and illustrated in Fig. 1. Similar calculations have been carried out for the Ni^{2+}/Ag interaction and the results were found to fit a Buckingham potential of the form

$$V(r) = 1473.1 \exp(-r/0.3247)\,\text{eV}.$$

Here the distance is measured in Å. This potential, along with the Mg^{2+}/Ag potential calculated for the earlier work, is plotted in Fig. 2. We note that the Ag/Ni^{2+} potential is slightly less repulsive than the Ag/Mg^{2+} potential, which is consistent with the smaller size of the Ni^{2+} ion.

In addition to the interaction between the ionic and metal cores, it is necessary to include a repulsive interaction to represent the energy required to embed the ions in the metal jellium. The energy of various neutral atoms embedded in a jellium of density n has been estimated by Puska [13]. The neutral atom with the closest electronic structure to the Ni^{2+} ion is the Fe atom, with an energy of the form

$$\Delta E = 0.338 + 932.32n + 2.288 \times 10^4 n^2 - 5.19 \times 10^5 n^3 + 5.35 \times 10^6 n^4. \quad (1)$$

Here n represents the electron density of the jellium in atomic units.

The density of electrons near the surface of a jellium has been estimated by Smith [14], using a free electron model. He chooses a solution of the form

$$n = (n_+/2)e^{-\beta z} \quad (2)$$

for the electron number density and calculates the parameters n_+ and β. Here z is the distance from the jellium edge. The values calculated for Ag were $n_+ = 8.73 \times 10^{-3}$ a.u. and $\beta = 1.23$ a.u. Combining equations (1) and (2), and neglecting the constant term in (1), gives us an estimate of the repulsive potential associated with embedding the Ni^{2+}ions in the jellium

$$\Delta E = 4.07e^{-z/0.43} + 0.506e^{-z/0.215}.$$

Here the energies are in eV and the distances are in Å. Higher order terms in the expression are too small to be significant. The energy associated with embedding the O^{2-} ion in the jellium was estimated previously, using the immersion energy for the Ne atom

$$\Delta E = 2.63e^{-z/0.43} + 0.602e^{-z/0.215}.$$

The immersion potential is a repulsive interaction and its magnitude is constant in the plane parallel to the interface. It helps to stabilize the interface by resisting motion of the ions into the spaces between the metal atoms.

The MIDAS code was modified to include the screened image interactions and the immersion potential and used to model the (100) Ni/Ag interface. The first four planes of the oxide were relaxed explicitly to equilibrium and a further ten planes were relaxed as a rigid block, representing an infinite half space of NiO. The metal cores were fixed and assumed to have the same lattice parameter as NiO (4.17 Å) as this maintains the periodicity of the NiO surface. The actual lattice parameter of Ag is 4.21 Å and in a real interface we would expect regions of near perfect fit separated by dislocation arrays. We are, therefore, modelling the region between the misfit dislocation array.

2.2. The calculated structure and energy of the interface

The interactions discussed above were used with the MIDAS code to calculate the structure and energy of the NiO/Ag interface. The work of adhesion of the interface, defined here as the difference between the calculated surface energy and the interfacial energy, is summarized in Table 1. Also included in the table are the equivalent results for the MgO/Ag interface. We note that our definition of the work of adhesion neglects the relaxations of the metal at the interface and at the free surface, as the metal cores are fixed in the calculation. The difference between the structure of the real metal at the surface and at the interface introduces a small degree of uncertainty into our calculations. Nevertheless, the results give an indication of the relative energies of the configurations for the NiO/Ag interface and a direct comparison with the MgO/Ag case.

It is clear from Table 1 that the work of adhesion is significantly larger for the NiO/Ag interface than for the MgO/Ag interface, leading to smaller wetting angles in the NiO case. This is a direct result of the smaller repulsive potentials of Ni/Ag. In both the MgO and NiO the lowest energy configuration was found to be the metal-over-cation case. This is in contrast to the LDA calculations which found the metal-over-oxygen configuration to have lower energy in MgO. Our result is sensitive to the calculated potential and a small reduction in the magnitude of the interaction energy between the O ion and the Ag

Table 1. The work of adhesion (in eV per unit cell), the dilation (the distance between the outer oxide plane and the metal in units of the interionic distance of NiO) and the calculated wetting angles for the NiO/Ag and MgO/Ag interfaces, with various lateral displacements

	NiO/Ag			MgO/Ag		
Interface	Work of adhesion	Dilation	Wetting angle	Work of adhesion	Dilation	Wetting angle
Over O	0.46	1.17	109°	0.32	1.2	123°
Over Mg/Ni	0.78	1.22	83°	0.62	1.3	98°
Interstitial	0.66	1.20	93°	0.48	1.2	108°

The wetting angles quoted are for the non-defective interface. Including defects in the second oxide plane reduces the NiO/Ag wetting angle to 52°.

Table 2. The calculated relaxations at a NiO/Ag interface

	Metal-over-O			Metal-over-Mg		
	Unrelaxed coordinates	Relaxed coordinates Cation	Anion	Unrelaxed coordinates	Relaxed coordinates Cation	Anion
Metal	−1.17			−1.22		
Plane 1	0.0	−0.002	−0.016	0.0	+0.014	−0.027
Plane 2	1.0	1.0–0.009	1.0–0.009	1.0	1.0–0.008	1.00–0.004

Distances are in units of the interionic distance of NiO (2.084 Å) and negative relaxations indicate movement of the oxide ions towards the metal. The relaxations refer to the core co-ordinates as these are normally measured. The dipole moments for all ions in the outer oxide plane were found to be negative.

atom in the tail of the potential could reverse the relative magnitudes of the configurations. Both configurations are seen experimentally in MgO [15], therefore it is likely that there is a fine balance between the energies in a real interface.

The relaxations which occur at the interface are summarized in Table 2. The coordinates are given relative to the unrelaxed positions of the outer oxide plane, in units of the NiO interionic distance (2.084 Å), and the positive direction is towards the oxide. The anion moves towards the metal more than the cation, due to the attractive nature of the potential between the metal atoms and the oxygen ions at the interfacial distances. Similar rumpling has been seen at free surfaces in oxides and it has important consequences defect concentrations near MgO surfaces [16].

3. POINT DEFECT ENERGIES

3.1. The calculation method

The energies of point defects near metal/oxide interfaces can be calculated using a modified version of the Harwell CHAOS code [17], which has been used to calculate point defect energies near oxide surfaces [10] and grain boundaries [9]. The modifications involve including image interactions and immersion energies as described in the earlier paper [1]. The relaxed structure of the interface is calculated using the Harwell MIDAS code and point defects are introduced into this reference configuration. The ions around the defect are relaxed explicitly and the displacements of the outer ions are calculated using a continuum electrostatic approach. Most of our calculations involved an inner region size of 100 ions. Some instabilities were found, particularly for cation vacancies near the metal-over-Mg interface, where the anions tended to move into the metal. We conclude that the displacements in these cases are too large to be treated with our atomistic method. As the anions approach the metal it is possible that a significant degree of charge transfer occurs. Such charge transfer requires electronic structure calculations (LDA for example) and are beyond the scope of our current model. All vacancies were, however, found to be stable in the metal-over-O configuration, and the point defect energies quoted in the next section refer to this configuration.

3.2. Point defect energies

The energies of cation and anion vacancies near the NiO/Ag interface, in the metal-over-O configuration, have been calculated and the results presented in Fig. 3. We note a similar behaviour to the results calculated for the MgO/Ag interface, in that the anion vacancy energies are significantly higher than the

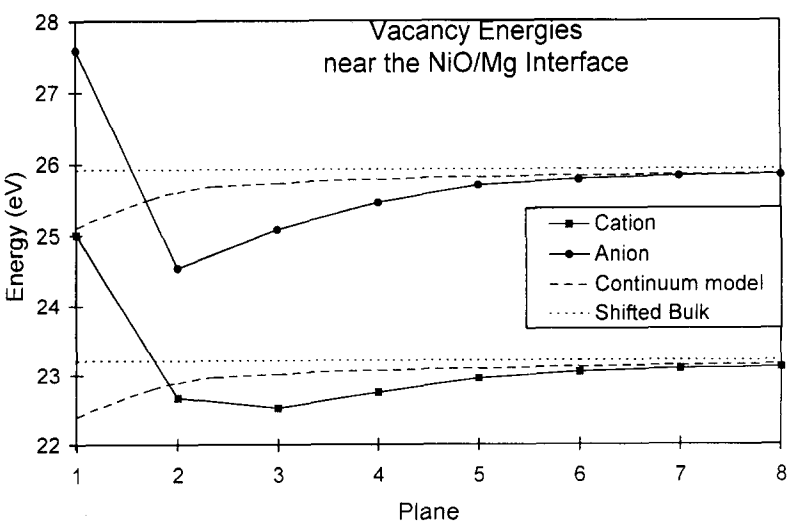

Fig. 3. The calculated energies of cation and anion vacancies near the Ag/NiO interface. The bulk vacancy energies, shifted by the interfacial potential, and the energy calculated using the continuum electrostatic model ($E_{\text{bulk}} - q^2/4\epsilon_0\epsilon_r z$), are included in the plot.

Table 3. A comparison between the calculated vacancy energies (eV) near the NiO/Ag interface and the MgO/Ag interface

	Cation vacancies		Anion vacancies	
	NiO	MgO	NiO	MgO
Bulk	24.43	24.41	24.70	24.94
Plane 1	25.01	22.09	27.59	24.89
Plane 2	22.66	20.87	24.54	24.20
Plane 3	22.52	21.76	25.08	24.98
Plane 4	22.75	22.65	25.45	25.70

cation vacancy energies. This effect originates from the rumpling of the interfacial ions mentioned in Section 2. The rumpling effectively introduces a dipole layer at the interface, which produces a potential shift of +0.61 V in the bulk oxide. Such a shift favours defects with a negative net charge, hence the energy of cation vacancies is reduced and that of anion vacancies is increased, relative to the bulk value. The continuum electrostatic result is also included in Fig. 3. This is the energy of a point charge near the interface between an oxide and a metal in the dielectric continuum limit. The total energy in this case is the bulk vacancy energy, shifted by the interfacial potential, plus the image energy, given by

$$E_{\text{image}} = -q^2/4\epsilon_0\epsilon_r z.$$

Here q is the net defect charge, ϵ_r is the relative dielectric constant of NiO (calculated from our potentials to be 12.63) and z is the distance between the defect and the image plane. We note that, from about the seventh oxide plane from the interface, the classical continuum gives a good description of the defect energy. Closer to the interface the atomistic nature of the interface is significant. In particular, the defect energy in the outermost oxide plane is very high, higher even than the bulk defect energy. This is a result of the reduced number of neighbours of a vacancy in this position. The short range energy gained by introducing a vacancy is reduced in the outer plane by the smaller number of neighbours, and the energy gain from relaxation is also reduced. In addition, the image energy of the defect suffers significant screening, due to the finite Fermi wavevector of the metal, in the outermost plane. The magnitude of the unrelaxed image energy is reduced by about 1.5 eV by the screening effect in the first plane whereas screening is negligible in the second plane. Thus the screening of the image energy also contributes to the higher vacancy energy of the outer plane. In all other planes the energy is lower than the continuum result, as the relaxations in the atomistic model are greater than the linear relaxations predicted by continuum theory. This emphasizes the necessity of going beyond continuum theory when considering defects close to interfaces.

Table 4. The calculated substitutional energies (eV) for Ni^{3+} and Ni^{+} ions near the NiO/Ag interface

Plane	Ni^{+} Energy	Ni^{3+} Energy
1	−29.97	18.33
2	−30.47	17.80
3	−30.12	17.83
4	−30.12	17.84
5	−30.04	17.90
6	−30.03	17.93
7	−30.02	17.94
Bulk	−30.61	18.58
Shifted bulk	−30.00	17.97

The defect energies are compared with the calculated energies at the MgO/Ag interface in Table 3. We note that, in spite of the fact that the structure and lattice parameters of the two materials are very similar, the vacancy energies are quite different. The magnitude of the image energy is expected to be less in NiO because of the higher dielectric constant (12.63 in NiO compared to a value of 8.0 for the rigid ion potentials used to model MgO). The higher dielectric constant produces more effective screening between the defect charge and the induced image charge, and the resulting reduced image energy leads to a higher net defect energy.

The lower ionization energies of the Ni^{2+} ion in NiO means that electronic disorder is possible in this oxide, where the charge state of the Ni^{2+} ion is increased or decreased by one electron. The energies of the Ni ion in the +1 and +3 charge states are summarized in Table 4. The Ni^{+} ion, with a negative net charge, has a lower energy at the interface than the equivalent bulk value and the Ni^{3+} ion has a higher energy. The energies converge towards the shifted bulk values as the defects move away from the interface and the outer planes have higher energies than expected, due to the reduced number of neighbours at these sites and the increased screening.

Table 5. The calculated energies (eV) of defect combinations at the NiO/Ag interface, in bulk NiO and at the NiO free surface

	Interface	Bulk	Surface
Isolated vacancy ($V_{Ni}^{=}$)	22.52	24.43	24.72
Hole (h^{+})	−30.47	−30.61	−30.73
Singly charged vacancy (V_{Ni}^{-})	−7.30	−6.70	−6.62
Neutral vacancy (V_{Ni})	−37.38	−37.56	−37.65
$V_{Ni}^{=} + h^{+}$	−7.95	−6.18	−6.00
$V_{Ni}^{=} + 2h^{+}$	−38.42	−36.79	−36.72
$V_{Ni}^{=} + h^{+} = V_{Ni}^{-}$	+0.65	−0.52	−0.62
$V_{Ni}^{=} + h^{+} = V_{Ni}^{-}$	+0.39	−0.25	−0.31

The hole refers to an Ni^{3+} substitutional ion and a singly charged vacancy is a vacancy with a hole on the adjacent cation site. A neutral vacancy has two holes on cation sites next to the vacancy. The sum of the isolated defect values and the energies of tthe defect association reactions are also included.

The energies of a number of defect combinations near the interface have also been calculated and these are summarized in Table 5. The equivalent results for the free surface and the bulk oxide have been included. These results enable us to estimate the energy required to associate defects in the bulk, at the surface and at the interface. For example, the energy required to form a singly charged vacancy from an isolated, doubly charged vacancy and a hole ($V_{Ni}^{=} + h^{+} = V_{Ni}^{-}$) is endothermic at the interface (0.65 eV) but exothermic both at a free surface and in the bulk (-0.62 and -0.52 eV respectively). The energy required to form a neutral vacancy from a singly charged vacancy and a hole ($V_{Ni}^{-} + h^{+} = V_{Ni}$) is also endothermic at the interface and exothermic at the free surface and in the bulk oxide. This is the result we would expect from simple image theory as defects with a high net charge gain image energy near a metal interface but lose energy at a free surface, where the image energy has the opposite sign.

4. DEFECT CONCENTRATIONS

The point defect concentrations, under various conditions, can be estimated using the energies presented in the previous section.

4.1. The equilibrium concentration

The dominant defects in NiO, in the presence of an oxygen atmosphere, are cation vacancies compensated by localized holes, which can be represented by an excess positive charge on the Ni ion. The reaction responsible for the formation of such defects is the oxidation reaction, in which an oxide atom is absorbed from the atmosphere and gains electrons by reducing the charge state of two Ni ions, producing two holes

$$1/2O_2 = O^{=} + V_{Ni} + 2h^{+}.$$

The energy of this reaction is the sum of half the dissociation energy of the oxygen molecule (2.55 eV), the first and second electron affinities of oxygen (7.37 eV), twice the ionization energy of Ni (2×35.2 eV), the coherent energy of the NiO lattice (-41.8 eV) and the calculated vacancy and hole energies. The electron affinities, generally considered to be a source of uncertainty in such calculations, were taken from Stoneham *et al.* [18], who compared the calculated value for the energy of the oxidation reaction MnO with the experimental value. The comparison was then used to estimate the sum of the oxygen affinities. The calculated defect energies for bulk NiO are 24.43 eV for the vacancy and -30.61 eV for the hole, thus the calculated energy for the oxidation reaction is 1.73 eV in bulk NiO. The bulk defect concentration can be estimated for a temperature of 1000 K and an oxygen pressure of 1 atm to be $\exp(-1.73/3/0.86)$ or 1.1×10^{-3} vacancies per cation. The vacancy energy is 1.77 eV lower at the interface and the hole energy is 0.14 eV higher, therefore the energy of the oxidation reaction is 0.24 eV at the interface, with a corresponding vacancy concentration of 0.4 defects per ion at 1000 K. Clearly defect interaction energies would need to be considered at such high defect concentrations and these would effectively increase the defect energy. Nevertheless, under equilibrium conditions, we expect a high concentration of vacancies at the interface.

4.2. Fixed vacancies and mobile holes

The activation energy for vacancy motion in NiO is high (around 1.8 eV [19]), therefore the vacancy distribution is effectively fixed at low temperatures. Holes, on the other hand, are relatively mobile and these will reach the equilibrium distribution in reasonable time scales, particularly with the help of optical excitations. We note, however, that holes have a higher energy at the interface than in the bulk, due to the interaction of the positive charge with the interfacial potential. They will, therefore, tend to move away from the interface, leaving an excess of vacancies. The resulting space-charge layer counteracts the boundary potential, resulting in a zero bulk potential. The hole distribution can be estimated by solving Poisson's equation

$$d^2\phi(z)/dz^2 = -\rho(z)/\epsilon_r\epsilon_0. \tag{3}$$

The charge distribution (ρ) is related to the potential (ϕ) by the expression

$$\rho(z) = 2ec_0[-1 + \exp(-e\phi/kT)] \tag{4}$$

Here c_0 is the fixed vacancy concentration. Equation (3) and (4) can be combined to give a differential equation of the form

$$d^2\Phi(z)/dz^2 = \kappa^2(1 - e^{-\Phi}) \tag{5}$$

where $\kappa^2 = 2ec_0/\epsilon_r\epsilon_0 kT$ and $\Phi = \phi/kT$. Equation (5) can be integrated to give

$$d\Phi/dz = \sqrt{2}\kappa(z + e^{-z})^{1/2}. \tag{6}$$

It is necessary to carry out the second integral numerically, and the resulting potential is illustrated in Fig. 4. The total energy of the resulting hole distribution can be estimated from the expression

$$E = -1/2\int \rho(z)\phi(z)dz$$

and it is found to be small (0.003 eV). We conclude therefore that the redistribution of holes has very little effect on the energy of the NiO/Ag interface, but it will have the effect of cancelling the interfacial potential.

4.3. The charge transfer reaction

Another possible source of disorder in oxides such as NiO is the electronic disorder associated with the charge transfer reaction

$$2Ni^{2+} = Ni^{+} + Ni^{3+}.$$

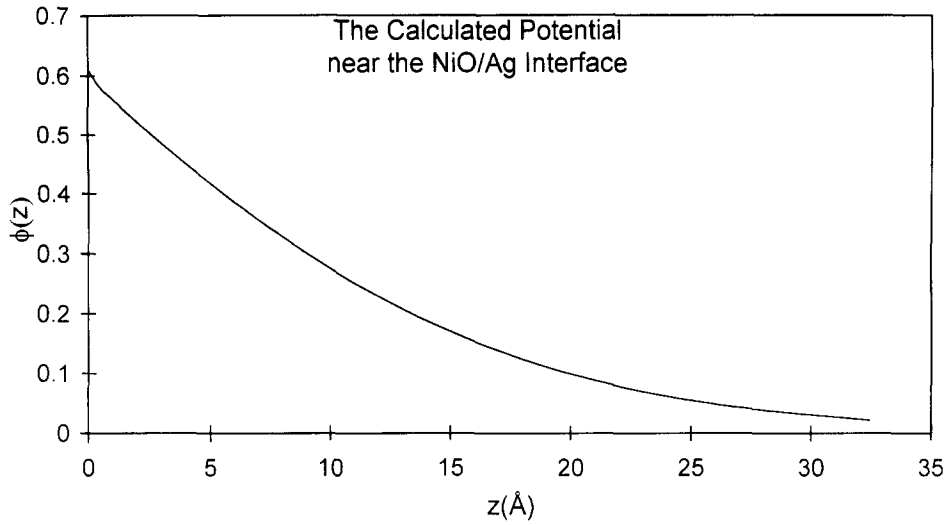

Fig. 4. The potential (ϕ) near the Ag/NiO interface, in the situation where vacancies are fixed and holes are mobile. The potential was calculated by integrated equation (6) numerically.

The total energy of the reaction is the sum of the first and second ionization energies of Ni, plus the substitutional energies of the Ni^{+} and Ni^{3+} ions in NiO. The sum of the substitutional energies was calculated to be -12.03 eV in bulk NiO and -12.67 eV at the interface. Adding these to the total ionization energy (17.1 eV) gives a total charge transfer energy of 5.1 eV in bulk NiO and 4.4 eV at the interface. Thus the reaction energy is too high to give any appreciable charge transfer in NiO. Other oxides which have lower ionization energies may experience charge transfer at a metal/oxide interface. One such oxide is FeO, where previous calculations have demonstrated the possibility of spontaneous charge transfer (negative U) at grain boundaries [20]. FeO has a total ionization energy of 14.5 eV, 2.6 eV lower than NiO. Thus we expect the energy of the charge transfer reaction to be around 1.7 eV at a FeO/metal interface. This is comparable with other defect energies, therefore an appreciable degree of electronic disorder may occur at a FeO/metal interface at elevated temperatures.

5. DEFECT ARRAYS

In the previous section we noted that the activation energy for the oxidation reaction is very low near the NiO/Ag interface and thus we expect a high concentration of defects. At such concentrations defects interactions become significant. One way to study the effect of defect interactions is to calculate the structure and energy of periodic arrays at defects using the MIDAS code. Initially we considered an interface with a unit cell four times the primitive unit cell, and introduced one neutral defect (1 vacancy + 2 holes) into each of these expanded unit cells. The configuration is illustrated in Fig. 5. The calculated energy of

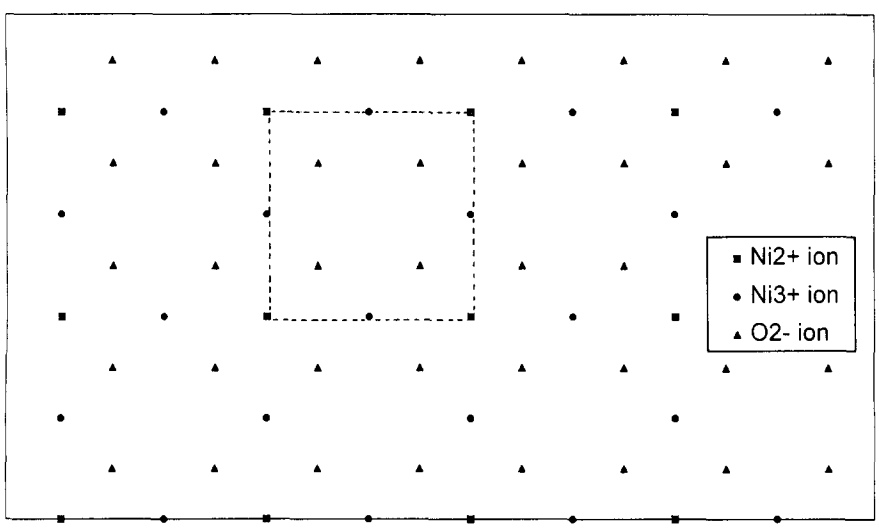

Fig. 5. The unrelaxed structure of the second oxide plane of the Ag/NiO interface which has one neutral defect in every four unit cells. The broken lines mark the surface unit cell.

such an interface was 35.92 eV per defect lower than the non-defective interface. Comparison with the energies in Table 5 reveals that this energy is higher than the neutral vacancy energy at the interface (−37.38 eV) therefore the interaction energy is positive in this configuration.

A second configuration was considered in which the cation sublattice of the second plane of oxide ions was saturated with defects. The basic unit cell was three times the primitive unit cell and each contained one neutral defect. The relaxation of this structure produced an energy of −38.77 eV per neutral defect, lower than the sum of the isolated defect energies at the interface. Thus, in this configuration the relaxation is such that the interaction energy between the defects at the interface is negative. The relaxed structure is illustrated in Fig. 6. The lines of O^{2-} ions move away from the negatively charged cation vacancies and towards the positively charged holes. This gives a structure in which columns of close packed ions are separated by large spaces. There is also significant relaxation in the plane perpendicular to the interface.

The total energy of the oxidation reaction at the interface for the saturated interface is calculated to be −0.11 eV, suggesting that this configuration has a lower energy than the non-defective interface. Similar interfaces, in which the lowest energy configuration appears to contain defects, have been found for the twist grain boundaries in NiO [21] and for the BaO/NiO interface [4]. In the NiO twist grain boundary the lowest energy configuration has a lower density of ions in the interfacial plane, equivalent to a regular array of Schottky defects. In the case of the BaO/NiO interface, the mismatch in the dielectric constants favours defects with a high net charge and a restructured configuration was found in which the two NiO planes nearest the interface contain cation vacancies and Ni^{3+} ions, similar to the NiO/Ag interface. The relative proportions of ions in the second oxide plane of the defective NiO/Ag interface correspond to an oxide with a higher proportion of oxygen than the normal oxide, i.e. Ni_2O_3. The oxygen rich (Ni_2O_3) oxide has been observed in a thin layer near a NiO/Ni interface [22], although we would normally expect the oxide to be metal rich near the metal interface. The structure described above, with a restructured plane of Ni vacancies and Ni^{3+} ions, could be the origin of such a phenomenon. A similar situation occurs for the FeO/Fe interface, where once again the oxygen rich (Fe_2O_3) oxide is observed [23] in a thin layer near the interface.

6. EXPERIMENTAL IMPLICATIONS

6.1. Wetting angles

The wetting angle (θ) of a metal on an oxide substrate is related to the surface energy of the oxide (γ_o), the metal (γ_m) and the energy of the interface between the two materials ($\gamma_{m|o}$), by the following expression

$$\cos\theta = (\gamma_o - \gamma_{m|o})/(\gamma_o).$$

The surface energy is defined as the difference between the energy of a block of material at the surface ($E_{m|}$) and an equivalent block in the bulk material (E_m). The interfacial energy is defined as the difference between the energy of a block of material at the interface ($E_{m|o}$) and the energy of the two blocks of material in the bulk

$$\gamma_{m|o} = E_{m|o} - E_{m.} - E_{.o}$$

which becomes

$$\gamma_{m|o} = E_{m|o} - \gamma_m - E_{.o}$$

in our calculations, because the metal is unrelaxed.

The parameters $E_{m||o}$, $E_{|o}$ and $E_{.o}$ are calculated by MIDAS and were found to be −167.84, −167.37 and −168.0 eV respectively, for the metal-over-O configuration. The experimental value for the surface

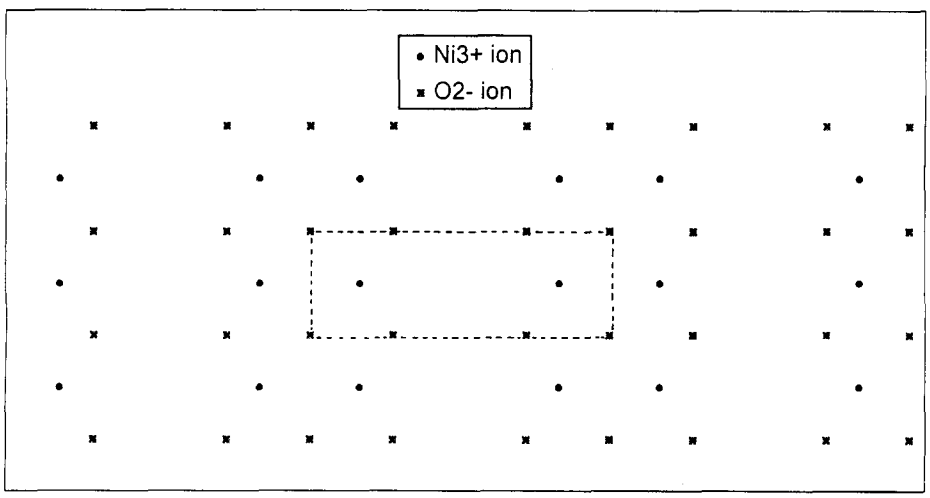

Fig. 6. The relaxed structure of the second oxide plane of the Ag/NiO interface with one neutral defect every three unit cells. The broken lines mark the expanded unit cell. The composition of this plane is equivalent to that of Ni_2O_3.

energy of Ag is 0.7 eV [24], therefore we estimate the wetting angle to be

$$\cos\theta = (0.63 - 0.86)/0.7$$
$$= 0.33$$
$$\theta = 109°.$$

This is the value quoted in Table 1. In the previous section we noted that an interface saturated with defects has a lower energy than the defect free interface, therefore such an interface should have a lower wetting angle. The defect energy (per neutral defect) is 1.98 eV lower at the interface than in the bulk, or 0.66 eV per unit cell. The wetting angle for the interface with defects becomes

$$\cos\theta = (0.63 - 0.2)/0.7$$
$$= 0.61$$
$$\theta = 52°.$$

Thus an array of defects at the interface dramatically reduces the wetting angle and it has the effect of changing a non-wetting interface into a wetting interface. In this wetting situation it is possible that the vacancies form by Ni ions dissolving in the metal. We are not aware of any experimental value for the wetting angle of Ag on NiO, however other metals exhibit much lower wetting angles on NiO than on MgO [25]. For example, the wetting angle of Cu is 160° on a MgO substrate and 68° on a NiO substrate. This difference is too large to be explained by the small difference in the interatomic potentials expected between the two ions.

6.2. *Strong-metal-support interactions*

It has been noted [26] that there is a strong correlation between wetting behaviour and Strong-Metal-Support Interactions (SMSI), in that oxides with a high dielectric constant tend to wet metals, and also exhibit SMSI. Strong-Metal-Support Interaction is the name given to the change in the catalyst morphology which occurs in some systems at high temperatures, under a reducing atmosphere [27]. In the situation where the reduced carrier has a stronger affinity with the metal than the oxidized carrier, the morphology changes in such a way that the catalyst behaviour is dramatically altered. Stoneham and Tasker [3] suggested that the introduction of charged defects during reduction contributed to the interfacial energy through the image interaction, and the subsequent increase in affinity with the metal was sufficient to cause the change in morphology. Indeed, we noted that arrays of defects at the NiO/Ag interface could change a non-wetting interface to a wetting interface, under certain conditions. The strong metal support interaction occurs at high temperatures, therefore we expect the defects to be mobile. It is possible that the oxide cations absorb electrons from neighbouring cations, forming holes, and dissolve in the metal. The oxide metal interface could then restructure to form a tightly bound interface of the type discussed above, and this may cause the observed changes in morphology.

7. CONCLUSIONS

We have modelled the interface between an oxide (NiO) and a metal (Ag), using well established simulation techniques, which have been modified to include the image interaction between the ionic charges and induced charge in the metal. The results were compared with those of previous calculations for the MgO/Ag interface which has a similar structure. Some similarities were noted, in particular the general behaviour of the vacancy energy near the interface. This was high on the interfacial plane, dropped significantly on the second and third planes, and converged to the continuum dielectric model at around the seventh ionic plane. The point defect energies, at both interfaces, were shifted by a potential difference introduced by the rumpling of the interfacial ions.

There were, however, significant differences between the two interfaces. These were related to the difference between the dielectric constants of the materials and the ease of formation of point defects. The oxidation defects (cation vacancies compensated by holes) which are present in NiO, but not MgO, introduce the possibility of the formation of a low energy structure in which the second ionic plane is saturated with defects. This plane restructures to form a configuration which has densely packed columns of ions separated by vacant columns. We predict that such an interface would have a low wetting angle due to the low energy of the defects at the interface relative to the bulk energy.

Thus we conclude that the image model, when combined with established modelling techniques, gives a good framework for understanding the general principles involved at metal/oxide interfaces. The detailed calculations on specific interfaces give reasonable agreement with other more complex calculations, and with experiment. Predictions can, therefore, be made about more complex interfaces which cannot be modelled in detail by our, or any other, approach.

REFERENCES

1. D. M. Duffy, J. H. Harding and A. M. Stoneham, *J. appl. Phys.* In press.
2. D. M. Duffy, J. H. Harding and A. M. Stoneham, *Phil. Mag. A* **67,** 865 (1993).
3. A. M. Stoneham and P. W. Tasker, *J. Physique* **C18,** L543 (1985).
4. A. M. Stoneham and P. W. Tasker, in *Ceramic Microstructures '86* (edited by J. A. Pask and A. G. Evans), p. 155. Plenum Press, New York (1987).
5. U. Schönberger, O. K. Andersen and M. Methfessel, *Acta metal. mater.* **40,** S1 (1992).
6. C. Li, R. Wu, A. J. Freeman and C. L. Fu, *Phys. Rev. B* **48,** 8317 (1993).

7. P. W. Tasker, A Guide to MIDAS, AERE Report No. R9130 (1978).
8. M. J. L. Sangster and A. M. Stoneham, *Phil Mag. B* **43,** 587 (1981).
9. D. M. Duffy and P. W. Tasker, *Phil. Mag. A* **50,** 143 (1984).
10. P. W. Tasker and D. M. Duffy, *Surf. Sci.* **137,** 91 (1984).
11. C. P. Wood and N. C. Pyper, *Molec. Phys.* **43,** 1376 (1981).
12. C. P. Wood and N. C. Pyper, *Phil. Trans. R. Soc. A* **320,** 71 (1986).
13. M. J. Puska, in *Springer Proceedings in Physics*, Vol. 48 (edited by R. M. Nieminen, M. J. Puska and M. J. Manninen), p. 134. Springer, Berlin (1990).
14. J. R. Smith, *Phys. Rev.* **181,** 522 (1969).
15. A. Trampert, F. Ernst, C. P. Flynn, H. F. Fischmeister and M. Ruhle, *Acta metal. mater.* **40,** S227 (1992).
16. D. M. Duffy, J. P. Hoare and P. W. Tasker, *J. Physique* **C17,** L195 (1984).
17. D. M. Duffy and P. W. Tasker, A Guide to CHAOS, AERE Report No. R1105 (1983).
18. A. M. Stoneham, S. M. Tomlinson, R. Catlow and J. Harding, in *Physics of Disordered Materials* (edited by D. Adler, H. Fritzche and S. R. Ovshinsky), p. 243. Plenum Press, New York (1985).
19. A. Atkinson and R. I. Taylor, *Phil. Mag. A* **43,** 979 (1981).
20. D. M. Duffy and A. M. Stoneham, *J. Physique* **C16,** 4078 (1983).
21. P. W. Tasker and D. M. Duffy, *Phil. Mag.* **47,** 145 (1983).
22. V. Dose, *Prog. Surf. Sci.* **13,** 225 (1983).
23. Y. Sakisaka, T. Miyano and M. Onchi, *Phys. Rev. B* **30,** 6849 (1984).
24. H. Wawra, *Z. Metallk.* **66,** 395.
25. J. V. Naidich, *Prog. Surf. Membr. Sci.* **14,** 354 (1981).
26. A. M. Stoneham, *Appl. Surf. Sci.* **14,** 249 (1982–83).
27. S. J. Tauster and S. C. Fung, *J. Catal.* **55,** 170 (1987).